Sensitivity limitations in optical speed meter topology of gravitational-wave antennas

S. L. Danilishin*
Department of Physics, Moscow State University, Moscow 119992, Russia
(Received 8 December 2003; published 27 May 2004)

The possible design of a quantum nondemolition gravitational-wave detector based on the speed meter principle is considered with respect to optical losses. A detailed analysis of a speed meter interferometer is performed and the ultimate sensitivity that can be achieved is calculated. It is shown that unlike with the position meter signal recycling can hardly be implemented in speed meter topology to replace the arm cavities, as is done in signal-recycled detectors such as GEO 600. It is also shown that a speed meter can beat the standard quantum limit by a factor of ~ 3 in a relatively wide frequency band, and by a factor of ~ 10 in a narrow band. For wideband detection the speed meter requires a quite reasonable amount of circulating power ~ 1 MW. The advantage of the considered scheme is that it can be implemented with minimal changes in the current optical layout of the LIGO interferometer.

DOI: 10.1103/PhysRevD.69.102003 PACS number(s): 04.80.Cc, 04.30.Db

I. INTRODUCTION

It is a well known fact that in order to detect gravitational waves very high precision devices are needed. The current technological progress in this area of knowledge suggests that a detector will achieve the level of sensitivity where its quantum behavior will play the main role.

The sensitivity of the third-generation interferometric gravitational wave detectors is planned to be higher than the standard quantum limit (SQL) [1,2]. Therefore, to overcome the SQL one needs to monitor not the coordinate of the detector probe body, as in contemporary detectors, but an observable that is not perturbed by the measurement. Such an observable has been called a quantum nondemolition (QND) observable [3–6]. One needs to monitor this kind of observable because, if there is no force acting upon the probe object, the observable value will remain unperturbed after the measurement. This means that there is no back action and, therefore, no SQL, limiting the sensitivity. In order to detect external action on the object it is reasonable to measure its integral of motion, which is a QND observable at the same time. For a free mass, its momentum can be that QND observable, but the realization of momentum measurement is not an easy task. In the article [7] it was proposed to measure the velocity of a free mass instead of momentum. Although it is not a QND observable and is perturbed during the measurement, it returns to its initial value after the measurement, and therefore can be used to beat the SQL. A device that measures the object velocity is called a speed meter.

The first realization of a gravitational-wave detector based on speed meter principle was proposed in [7]. In this article the authors suggested measuring the velocity of a free mass placed in a gravitational wave field. Analysis of the scheme has shown that measuring velocity instead of body coordinates allows the back action noise to be canceled and, therefore, significantly increases the scheme sensitivity. The measuring system was presented as two coupled microwave cavities whose coupling constant had to be chosen so that phase shifts proportional to the coordinate were fully compensated, while the output signal contained information about the probe mass velocity only.

Later, in [8] the possibility of applying the speed measurement technique to interferometric gravitational-wave detectors was analyzed. It was suggested to attach to the probe bodies of the detector small rigid Fabry-Pérot cavities. These cavities, fully transparent for light at a certain frequency ω_0 when immobile, introduce a phase shift in the output light due to the Doppler effect. By measuring this phase shift it is possible to measure the probe body velocity. It was shown in this article that the speed meter can potentially beat the SQL if the pumping power is larger than one for a SQL limited position meter: $W > W_{\mathrm{SQL}}$.

The realization of a speed meter based on two microwave coupled resonators, suggested in [7], was considered in [9]. This speed meter was proposed to be attached to the detector probe body to measure its velocity. It was demonstrated that it is feasible, with current technology, to construct such a speed meter that beats the SQL in a wide frequency band by a factor of 2. A possible design of a speed meter for an optical frequency band was also proposed. This design demands construction of four large scale cavities instead of two as in the traditional LIGO detector. The disadvantage of this scheme, common for all speed meters, is the extremely high power circulating in the cavities.

A further comprehensive analysis of the scheme proposed in [9] was carried in [10]. It was shown that *in principle* the interferometric speed meter can beat the gravitational-wave standard quantum limit by an arbitrarily large amount, over an arbitrarily wide range of frequencies, and can do so without the use of a squeezed vacuum or any auxiliary filter cavities at the interferometer's input or output. However, *in practice*, to reach or beat the SQL, this specific speed meter requires exorbitantly high input light power. The influence of losses on the speed meter sensitivity was also analyzed, and it was shown that optical losses in the considered scheme influence the sensitivity at low frequencies.

In [11,12] more practical schemes for large scale interferometric speed meters based on the Sagnac effect [13] were analyzed and proposed for use in possible design of

*Email address: stefan@hbar.phys.msu.ru

third-generation LIGO detectors. It should be noted that use of Sagnac interferometers in gravitational-wave detection was suggested earlier in [14–17]. In [11,12] it was shown that to lower the value of circulating power one should use the squeezed vacuum input with a squeezing factor of ~ 0.1, and variational output detection [18]. Then it is possible to beat the SQL by a factor of $\sim\sqrt{10}$. The schemes analyzed are based on using either three large scale Fabry-Pérot cavities [11] or ring cavities and optical delay lines [12]. A comprehensive analysis of the above mentioned schemes including optical losses was carried out.

Another variant of a Sagnac based speed meter was proposed in [19]. This design requires little change in the initial LIGO equipment and seems to be a good candidate for implementation. The scheme of the interferometer proposed in [19] is considered in this paper. We analyze here how this meter will behave when there are optical losses in the interferometer mirrors and obtain the optimal value of the circulating power and how it depends on cavity parameters.

This article is organized as follows. In Sec. II we consider the simple scheme of a speed meter with a single lossy element in order to study how optical losses influence the scheme sensitivity. In Sec. III we compare the sensitivities of a signal-recycled position meter and a speed meter, and demonstrate that the later has worse sensitivity at the same level of pumping power if signal recycling is applied. In Sec. IV we evaluate the sensitivity of the more realistic speed meter scheme proposed in [19] and obtain the optimal values of the parameters that minimize the influence of noise sources. In Sec. V we summarize our results.

II. SIMPLE SAGNAC SPEED METER SCHEME WITH OPTICAL LOSSES

A. Input-output relations for simple speed meter scheme

In this section we will analyze the action of a simple speed meter scheme based on the Sagnac effect to estimate how optical losses affect its sensitivity. This scheme is a model that is quite easy for analysis and yet contains all features specific for a speed meter. It differs from real, complicated schemes only in the fact that there is no bending up of the noise curve at high frequencies that arises due to the finite bandwidth of Fabry-Pérot cavities being used in real speed meter interferometers. Therefore, it seems convenient to investigate this simple scheme before analyzing complicated speed meters designed for LIGO.

The scheme we want to consider is presented in Fig. 1. Its action can be described as follows: the light beam from a laser enters the scheme from the ''western'' side of the figure and is divided by the beam splitter into two beams propagating in the ''northern'' and ''eastern'' directions. Each beam is reflected sequentially from two movable end mirrors. Between these reflections the beams are reflected from the central mirror. The end mirrors we suppose to be ideally reflective, while the central mirror has the amplitude reflectivity r and transmittance t. We suppose that all optical losses are concentrated in the central mirror and therefore can be expressed by a single parameter t. It can be shown that for gravitational-wave detectors this approximation is satisfied quite well.

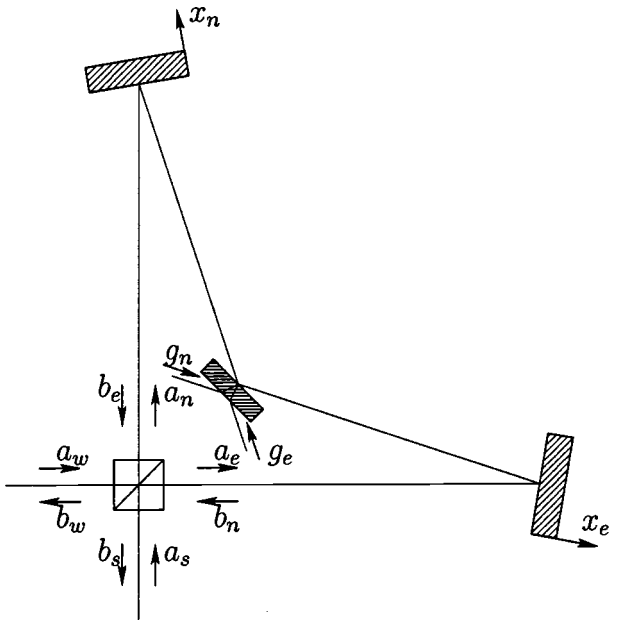

FIG. 1. Simplified scheme of speed meter.

After the three above mentioned reflections the light beams return to the beam splitter where they are mixed up. We suppose that the arm lengths are chosen so that all the light power returns to the laser. Then the photodetector located in the ''southern'' part of the figure will register only vacuum oscillations whose phase is modulated by the end mirror motion.

The input light can be presented as a sum of a classical pumping wave with frequency ω_0 and sideband quantum oscillations. The electric field strength of the incident wave can be written as

$$\hat{E}(t)=\ell(\omega_0)\{Ae^{-i\omega_0 t}+A^*e^{i\omega_0 t}\}+\int_0^\infty \ell(\omega)[\hat{a}(\omega)e^{-i\omega t} + \hat{a}^\dagger(\omega)e^{i\omega t}]\frac{d\omega}{2\pi}, \quad (1)$$

where A is the classical wave quadrature amplitude, $\hat{a}(\omega)$ is the quantum fluctuation sideband operator, $\ell(\omega)=\sqrt{2\pi\hbar\omega/\mathcal{A}c}$ is a normalization factor, and $\mathcal{A}$ is the beam cross section. Using this formalism we can write down input-output relations for the scheme. The incident wave quadrature amplitude and fluctuations we will denote as A and $\hat{a}_w$ as they come from the ''western'' side of the figure. Zero oscillations entering the scheme from the ''southern'' side we will denote as $\hat{a}_s$. After the beam splitter we will have two light beams propagating in the ''northern'' and ''eastern'' directions. These beam values we will mark by indices ''n'' and ''e,'' respectively. Moreover, there is a transparent central mirror that is the source of additional noise denoted as $\hat{g}_n$ and $\hat{g}_e$ (see Fig. 1).

TABLE I. Expressions for values used in Sec. II.

$x_-(\omega_0-\omega)$	$\frac{x_e-x_n}{2}$
$\hat{g}_s$	$\frac{i\hat{g}_e-\hat{g}_n}{\sqrt{2}}$
$\kappa(\omega)$	$\sqrt{\omega\omega_0}/c$
β_{input}	$ire^{4i\omega\tau}$
β_{loss}	$-ite^{2i\omega\tau}$
$\mathcal{K}_{simple}$	$-2\kappa(\omega)A(ire^{i(\omega_0+3\omega)\tau}-\eta e^{i(\omega_0+\omega)\tau})$
P_{simple}	$\frac{16\omega_0 W\tau^2}{mc^2}$

Let us denote the beam that travels in the interferometer arm for the first time as the ''primary'' beam, while the same beam that has left its first arm and entered the second one we will denote as the ''secondary'' beam. Due to absorption, the powers of the primary and secondary beams relate to each other as $W_{secondary}/W_{primary}=r^2=1-\alpha_{loss}^2$, where α_{loss} is the interferometer absorption coefficient. This coefficient is quite small and in practice can be neglected for the values of the classical powers but, in principle, there is an opportunity to compensate these losses by introducing some additional power into arms. This opportunity can be taken into account by assuming $W_{secondary}/W_{primary}=\eta^2$, where η is some coefficient that is equal to $1-\alpha_{loss}^2$ without additional pumping, and can be larger with it. We will assume that $\eta=1$ as optical losses in the considered schemes are supposed to be very small ($\alpha_{loss}\sim 10^{-5}$). Then the output wave can be written as (see Appendix A)

$$\hat{b}_s=\beta_{input}\hat{a}_s+\beta_{loss}\hat{g}_s+\mathcal{K}_{simple}x_-. \tag{2}$$

Expressions for β_{input}, β_{loss}, $\mathcal{K}_{simple}$, x_-, and $\hat{g}_s$ are summarized in Table I.

B. Quantum noise spectral density

In order to evaluate the scheme sensitivity we need to calculate the spectral density of total quantum noise. Suppose the mirror dynamics can be described by a free body equation of motion, i.e.,

$$m\ddot{x}=F.$$

Here $F=F_{\rm GW}+F_{fluct}$, where $F_{\rm GW}$ is the gravitational-wave force measured, F_{fluct} is the fluctuational force that arises due to radiation pressure of the incident light, and $x=x_{\rm GW}+x_{fluct}$ is the mirror displacement that consists of displacement due to gravitational-wave action and a noisy part that arises due to incident light phase fluctuations. The total noise spectral density then can be written as

$$S(\Omega)=S_F(\Omega)+m^2\Omega^4S_x(\Omega)-2m\Omega^2\Re[S_{xF}(\Omega)], \tag{3}$$

where Ω is the observation frequency, and $S_x(\Omega),S_F(\Omega),S_{xF}(\Omega)$ are the spectral densities of fluctuational mirror displacement x_{fluct}, fluctuational radiation pressure force F_{fluct}, and their cross correlation, respectively.

In our specific case these spectral densities are equal to (see Appendix A)

$$S_F(\Omega)=\frac{8\hbar\omega_0 W}{c^2}\cdot[1-r\cos(2\Omega\tau)], \tag{4a}$$

$$S_x(\Omega)=\frac{\hbar c^2}{16\omega_0 W\sin^2\Psi}\cdot\frac{1}{1+r^2-2r\cos(2\Omega\tau)}, \tag{4b}$$

$$S_{xF}(\Omega)=-\frac{\hbar}{2}\cot\Psi. \tag{4c}$$

Here W is the pumping power at the end mirrors, and Ψ is the homodyne angle that allows us to minimize the value of Eq. (3) significantly. This angle is chosen so that one measures not the amplitude or phase quadrature component but their mixture. This principle provides the basis for the variational measurement technique [18,20]. Here Ψ is one of the optimization parameters that allows one to overcome the SQL when chosen in the proper way.

Suppose that the signal varies slowly compared to the scheme characteristic time τ, and, therefore,

$$\Omega\tau\ll 1, \tag{5a}$$

$$\Omega\ll\frac{2\pi}{\tau}, \tag{5b}$$

where $\tau=L/c$, and L is the distance between the central and end mirrors. These assumptions we will call the *narrowband approximation*. Later we will see that for real detectors this approximation works pretty well.

Using this approximation we can rewrite Eqs. (4) as

$$S_F(\Omega)=\frac{8\hbar\omega_0 W}{c^2}\cdot[1-r+2r(\Omega\tau)^2], \tag{6a}$$

$$S_x(\Omega)=\frac{\hbar c^2}{16\omega_0 W\sin^2\Psi}\cdot\frac{1}{(1-r)^2+4r(\Omega\tau)^2}, \tag{6b}$$

$$S_{xF}(\Omega)=-\frac{\hbar}{2}\cot\Psi. \tag{6c}$$

If we substitute the expressions obtained in Eq. (3) and divide by the value of the radiation pressure noise SQL spectral density for the free mass $S_{SQL}=\hbar m\Omega^2$, we will obtain the factor by which the speed meter beats the SQL:

$$\xi^2=\frac{1}{2}\left[\frac{P_{simple}}{(\Omega\tau)^2}\cdot[1-r+2r(\Omega\tau)^2]+\frac{(\Omega\tau)^2}{P_{simple}}\frac{2(1+\cot^2\Psi)}{(1-r)^2+4r(\Omega\tau)^2}+2\cot\Psi\right]. \quad (7)$$

The expression for P_{simple} is presented in Table I.

The main goal of optimization is to beat the SQL in a frequency band that is as wide as possible. First of all we should find the optimal value of $\cot\Psi$ and P_{simple}. These parameters should not depend on frequency; therefore we will optimize them at high frequencies, i.e., $\Omega\tau\to\infty$. This optimization will result in the following values:

$$\cot\Psi=-2rP_{simple}, \quad (8)$$

and being substituted in Eq. (7) will produce

$$\xi^2_{\rm HF}\simeq\frac{1}{4rP_{simple}}. \quad (9)$$

Obviously, the rise of ξ^2 at low frequencies is determined by the radiation pressure spectral density as all other items in Eq. (3) are proportional to Ω^2 and Ω^4 and, therefore, cannot influence at low frequencies. Hence we see that optical losses lead to a decrease of speed meter sensitivity when the observation frequency is small. It is useful to calculate the value of the parameter P_{simple} that provides the minimum of ξ^2 at the defined frequency Ω^*. It can be shown that for $1-r\ll1$ this value is equal to

$$P^{opt}_{simple}\simeq\frac{\Omega^*\tau}{\sqrt{2(1-r)}}. \quad (10)$$

One can also readily obtain the minimal frequency where the speed meter sensitivity is equal to the SQL, i.e., where $\xi^2=1$ is satisfied, is defined by the expression

$$\Omega_{min}\simeq\frac{P_{simple}\sqrt{2(1-r)}}{\tau\sqrt{4P_{simple}-1}}, \quad (11)$$

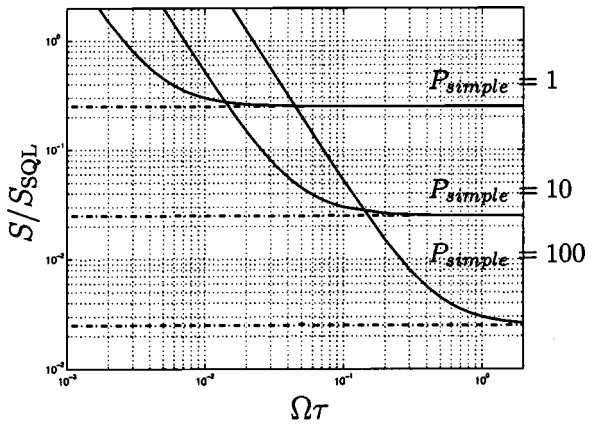

FIG. 2. Typical curves for $\xi^2=S/S_{SQL}$ at different P_{simple}.

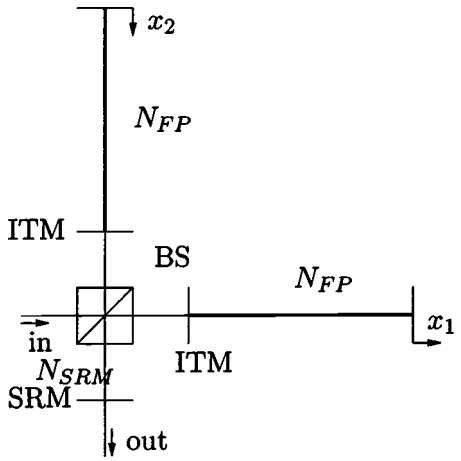

FIG. 3. Signal-recycled position meter.

where r is the central mirror amplitude reflectivity coefficient that characterizes the scheme optical losses. Here we suppose $t\ll1$.

Comparison of the expressions (9) and (11) shows that one needs to increase the optical power ($P_{simple}\to\infty$) in order to obtain high sensitivity, while to have a wide frequency band and increase the sensitivity at low frequencies it is necessary to have a low value of the pumping power to decrease radiation pressure noise. In Fig. 2 several curves are presented that demonstrate how ξ^2 depends on the frequency at different values of P_{simple}. The dot-dashed lines are for the ideal case where losses are equal to zero ($r=1$).

III. SIGNAL-RECYCLED SPEED METER VS SIGNAL-RECYCLED POSITION METER

In this section we will consider semiqualitatively the influence of a signal-recycling mirror on the sensitivity of the traditional position meter and speed meter. Let us consider the two schemes presented in Figs. 3 and 4.

Suppose $T_{FP}\sim1/N_{FP}$ and $T_{SRM}\sim1/N_{SRM}$ are the trans-

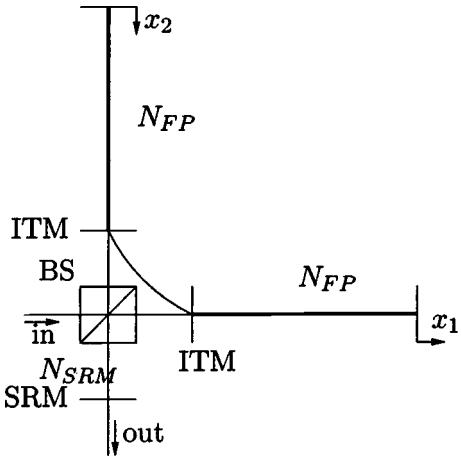

FIG. 4. Signal-recycled speed meter.

mittances of the arm cavity input mirrors (ITMs) and signal-recycling mirrors (SRMs), respectively. Here N_{FP} shows how many times the light beam is reflected from the end mirrors until it leaves the cavity, and N_{SRM} is the number of light beam reflections from the SRM before leaving the whole scheme. The first number characterizes the Fabry-Pérot half bandwidth, while the second one represents the signal-recycling cavity half bandwidth. Let τ be the time the light needs to travel from one cavity mirror to another. Suppose also the mirror motion is uniform and can be expressed during the light storage time ($\tau^* \sim N_{FP}N_{SRM}\tau < \tau_{GW} \sim \pi/\Omega_{GW,max}$) by the formula

$$x_i = x_{i,0} + v_i t,$$

where the subscript $i=1,2$ denotes the interferometer arm, $x_{i,0}$ are the end mirror initial positions, and v_i are their velocities.

In the case of the position meter the light path is the following. After leaving the beam splitter light enters both cavities, it passes from one arm cavity mirror to another $2N_{FP}$ times, then it is reflected from the SRM and returns to the cavity. This cycle repeats N_{SRM} times until the light leaves the scheme and goes to the homodyne detector. The output beam phase shift in our simple case can be written as

$$\delta\varphi_{signal} \simeq \frac{2\omega_0}{c} N_{FP}N_{SRM}\bar{x}_-, \tag{12}$$

where $\bar{x}_- = \bar{x}_1 - \bar{x}_2$ is the mean end mirror relative displacement during the storage time, and c is the speed of light.

As for the speed meter, the light path in this scheme differs from the previous one. Light that leaves, for example, the first cavity goes not to the beam splitter and then to the SRM, but to the second cavity, where it experiences N_{FP} reflections from the end mirror in addition to those in the first cavity. Then it is reflected from the SRM and so on for N_{SRM} times until it leaves the scheme. It can be shown that in this specific case the output beam phase shift will be written as

$$\delta\varphi_{signal} \simeq \frac{2\omega_0}{c} N_{SRM}N_{FP}^2\bar{v}_-\tau, \tag{13}$$

where $\bar{v}_- = \bar{v}_1 - \bar{v}_2$ is the relative velocity of the end mirrors.

We can readily see that the position meter and speed meter output signals depend on the arm cavity (N_{FP}) and signal-recycling cavity (N_{SRM}) parameters in different ways. It can be shown that this difference significantly influences the sensitivity of these schemes. Let us calculate the amount of circulating optical power necessary to achieve the level of SQL in each of the above mentioned schemes. The output signal field quadrature component a_{signal} for both schemes is proportional to the product

$$a_{signal} \simeq A\,\delta\varphi_{signal},$$

where A is the input radiation field quadrature amplitude. Therefore the spectral density of the phase fluctuations can be expressed in terms of the spectral density of a_{signal} as

$$S_\varphi = \frac{S_a}{|A|^2}.$$

The expression for S_a can be readily obtained and is equal to

$$S_a = \frac{1}{4},$$

and $|A|^2$ can be represented in terms of the power circulating in the arms as

$$|A|^2 = \frac{W}{\hbar\omega_0 N_{FP}N_{SRM}}.$$

Then for S_φ one will have the following expression:

$$S_\varphi = \frac{\hbar\omega_0 N_{FP}N_{SRM}}{4W}. \tag{14}$$

On the other hand, for the position meter this spectral density can be expressed in terms of the mirror displacement spectral density caused by radiation shot noise corresponding to the SQL, $S_x^{SQL} = \hbar/m\Omega_0^2$, as

$$S_\varphi^{PM} = \frac{4\omega_0^2 N_{FP}^2 N_{SRM}^2}{c^2} S_x^{SQL} = \frac{4\hbar\omega_0^2 N_{FP}^2 N_{SRM}^2}{mc^2\Omega_0^2}, \tag{15}$$

where Ω_0 is some fixed observation frequency, m is the mirror mass, and for the speed meter in terms of the mirror velocity spectral density caused by radiation shot noise corresponding to the SQL $S_v^{SQL} = \hbar/m$ as

$$S_\varphi^{SM} = \frac{4\omega_0^2\tau^2 N_{FP}^4 N_{SRM}^2}{c^2} S_v^{SQL} = \frac{4\hbar\omega_0^2\tau^2 N_{FP}^4 N_{SRM}^2}{mc^2}. \tag{16}$$

Substituting Eq. (14) into Eqs. (15) and (16) we will obtain the following values of the circulating power for both schemes considered:

$$W_{PM} = \frac{mc^2\Omega_0^2}{16N_{FP}N_{SRM}\omega_0}, \quad W_{SM} = \frac{mc^2}{16N_{FP}^3 N_{SRM}\omega_0\tau^2}. \tag{17}$$

If we divide W_{SM} by W_{PM} we will obtain the factor of χ by which the speed meter circulating power necessary to achieve the SQL is larger than that for the position meter:

$$\chi = \frac{W_{SM}}{W_{PM}} = \frac{1}{(N_{FP}\Omega_0\tau)^2} \gg N_{SRM}^2, \tag{18}$$

where we have taken into account that the light storage time should be much smaller than the period of the gravitational wave, i.e., $\tau^* \sim N_{FP}N_{SRM}\tau \ll \pi/\Omega_0$. Obviously, the above estimates show that a speed meter with signal recycling can hardly be considered as the best variant for implementation as a QND meter, as it requires much more circulating power than the signal-recycled position meter with the same param-

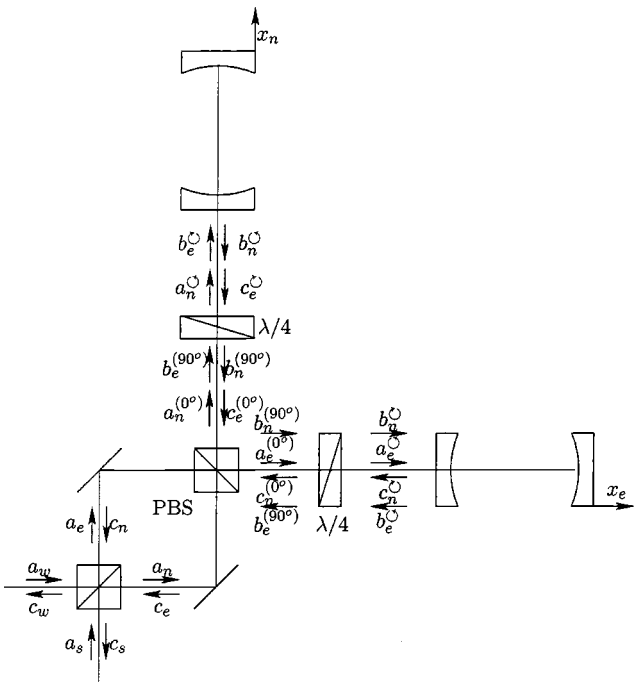

FIG. 5. Speed meter interferometer.

eters. More precise calculations that prove the above simple considerations are performed in Appendix B.

IV. OPTICAL LOSSES IN SPEED METER INTERFEROMETERS WITH FABRY-PÉROT CAVITIES IN ARMS

A. Speed meter interferometer action and output signal

Let us consider the scheme of a gravitational-wave detector based on the speed meter principle presented in Fig. 5. This interferometer differs from the traditional LIGO interferometers by an additional polarization beam splitter (PBS) and two quarter-wave plates ($\lambda/4$). Quarter-wave plates are needed to transform the input light polarization from linear ($0°$ and $90°$) to circular ($\circlearrowleft$ and $\circlearrowright$) during each pass. After reflecting from one of the 4 km long Fabry-Pérot (FP) cavities the light polarization varies over $90°$, and the light beam is reflected from the PBS to the second FP cavity. Hence, the light beam passes not only one FP cavity, but both cavities in sequence. As there are two beams that propagate in opposite directions (in clockwise and counterclockwise directions, respectively) the scheme output does not contain any information about the symmetric mechanical mode of the mirrors, i.e., about the sum of the end mirror displacements. This mode is not coupled with a gravitational-wave signal, and its presence can significantly lower the sensitivity and prevent it from beating the SQL. The output signal of this scheme can be found in the same manner as was done in [19]. The only problem is to include additional types of noise, arising due to internal losses in the optical elements, in the calculations. To do so, suppose each mirror to be a source of two independent additional types of noise, that stand for the interaction of electromagnetic radiation with the mirror medium excitations. This approach is based on the Huttner-Barnett scheme [21] of electromagnetic field quantization in linear lossy dielectrics. Using this approach one can obtain input-output relations for any optical device with losses (see [22–24]).

It should also be noted that we do not consider the beam splitters, polarization (PBS) and ordinary (BS), and quarter-wave plates as separate sources of additional noise that arise due to their internal losses. The reason is that the laser beam interacts with these optical elements $N_{eff}=2/|\ln r_1 r_2| \simeq 2/1-r_1 r_2 \sim 10^2$ times more seldom than with the Fabry-Pérot cavity mirrors (here N_{eff} is the effective number of laser beam reflections from the FP cavity mirrors). Therefore, the contribution of these elements to the total optical loss coefficient will be N_{eff} times smaller than that for the FP mirrors, and can be neglected.

Let us use the same notations as in Sec. II for the scheme parameters. In order to distinguish values that correspond to inner and end mirrors we will denote the first ones by the subscript 1 and the second ones by the subscript 2. Each Fabry-Pérot cavity has the following parameters: the mirror reflectivity, transmittance, and absorption coefficients are equal to $-r_1, -r_2$, it_1,0, and ia_1, ia_2, respectively, and the cavity length is L. The end mirror transmittance we suppose to be equal to zero because there is no difference whether the light exits or is absorbed in the end mirror.

Suppose that the classical pumping wave amplitude is A and the sideband fluctuation operator is $\hat{a}_w$. Suppose also that zero oscillations that enter the scheme from the ''southern'' side are described by the operator $\hat{a}_s$. We will also need the operators $\hat{g}_{s_{11}}$, $\hat{g}_{s_{12}}$, $\hat{g}_{s_{21}}$, and $\hat{g}_{s_{22}}$ to describe noises due to internal losses in the FP mirrors (the second numerical subscript stands for the number of noise type that arise in the mirror due to internal losses). The superscripts I and II denote which types of noise arise during the first and the second reflection, respectively. The parameter η we assume to be equal to unity, where η has the same meaning as in the simple scheme and is equal to the ratio of the classical amplitudes inside the cavity during the second and the first reflection, respectively (see Appendix C).

Finally, we are able to write down the output sideband fluctuation operator $\hat{c}_s$ that contains information about the mirror movements, and therefore about the gravitational wave force:

$$\begin{aligned}\hat{c}_s = \frac{1}{\mathcal{L}^2(\omega)}\{ & i\mathcal{B}_1^2(\omega)\hat{a}_s^I(\omega) \\ & -[e^{2i\omega\tau} r_2 t_1 a_1 \hat{g}_{s_{11}}^I(\omega) + e^{i\omega\tau} t_1 a_2 \hat{g}_{s_{21}}^I(\omega)] \\ & - i\mathcal{L}(\omega)[e^{2i\omega\tau} r_2 t_1 a_1 \hat{g}_{w_{11}}^{II}(\omega) - e^{i\omega\tau} t_1 a_2 \hat{g}_{w_{21}}^{II}(\omega)]\} \\ & - \mathcal{K}_{SM} x_-(\omega_0 - \omega). \end{aligned} \tag{19}$$

The notation used in this expression is presented in Table II.

B. Speed meter spectral densities and sensitivity

Here we will obtain the expressions for radiation pressure noise and shot noise and their cross-correlation spectral den-

TABLE II. Expressions for values used in Sec. IV. Here E is the classical complex amplitude of the pumping field near the movable mirror after the first reflection.

	Exact form	Narrowband approximation
γ_1	—	$t_1^2/4\tau$
α	—	$\alpha_1+\alpha_2=\frac{a_1^2+a_2^2}{4\tau}$
γ	—	$\gamma_1+\alpha=\frac{1-r_1 r_2}{2\tau}$
W	$\hbar\omega_0\lvert E\rvert^2/4$	$\hbar\omega_0\lvert E\rvert^2/4$
$\mathcal{L}(\Omega)$	$r_1 r_2 e^{2i\Omega\tau}-1$	$2\tau(\gamma+i\Omega)$
$\mathcal{B}_1(\Omega)$	$r_1-e^{2i\Omega\tau}r_2(r_1^2+t_1^2)$	$2\tau(\gamma-2\gamma_1+i\Omega)$
$\mathcal{K}_{SM}$	$-\frac{\kappa(\omega_0-\Omega)r_2 t_1[\mathcal{B}_1(\Omega)-\mathcal{L}(\Omega)]e^{i\Omega\tau}}{\mathcal{L}^2(\omega)}E$	$-\frac{2\kappa(\omega_0-\Omega)\sqrt{\gamma_1/\tau}(\gamma-\gamma_1+i\Omega)}{(\gamma+i\Omega)^2}E$

sities. We will suppose that the same additional pumping procedure as in Sec. II is taking place. Here we will use the same approximation that is defined by Eq. (5) of Sec. II. It is useful to evaluate if this approximation is valid for LIGO. The parameters for the LIGO interferometer are the following:

$$\omega_0=1.77\times10^{15}\ \mathrm{s}^{-1},\quad \tau=1.33\times10^{-5}\ \mathrm{s},$$

$$m=40\ \mathrm{kg},\quad L=4\times10^{3}\ \mathrm{m}.$$

If we suppose that the gravitational signal upper frequency is about $\Omega=10^3\ \mathrm{s}^{-1}$, then there remain no doubts that for LIGO the condition of the narrowband approximation applicability is satisfied as $\Omega\tau=1.33\times10^{-2}\ll1$.

One is able to obtain the following expressions for the spectral densities (see derivation in Appendix C):

$$S_x(\Omega)=\frac{\hbar L^2}{32\omega_0\tau W}\frac{(\gamma^2+\Omega^2)^2}{2\gamma_1\sin^2\Psi[(\gamma-\gamma_1)^2+\Omega^2]},\tag{20a}$$

$$S_F(\Omega)=\frac{8\hbar\omega_0\tau W}{L^2}\frac{\gamma(\gamma^2+\Omega^2)-\gamma_1(\gamma^2-\Omega^2)}{(\gamma^2+\Omega^2)^2},\tag{20b}$$

$$S_{xF}=-\frac{\hbar}{2}\cot\Psi,\tag{20c}$$

where Ψ is the homodyne angle, and W is the pumping power at the end mirrors. The expressions for γ_1 and γ are given in Table II.

One can obtain the result that the minimum force that can be measured by the speed meter presented in Fig. 5 depends on the total measurement noise spectral density. This spectral density can be expressed by the formula (3) with one exception: m in this formula is equal to one-fourth of the real end mirror mass. The multiplier 1/4 appears when we suppose not only the end mirrors to be movable, but also the inner ones.

Now we can write down the expression for $\xi^2=S_{SM}/S_{SQL}$, where S_{SM} is the total quantum noise of the speed meter that is calculated in accordance with Eq. (3), and $S_{SQL}=\hbar m\Omega^2$ is the SQL spectral density for the fluctuational force:

$$\xi^2=\frac{8\omega_0\tau W}{mL^2\Omega^2}\frac{\gamma(\gamma^2+\Omega^2)-\gamma_1(\gamma^2-\Omega^2)}{(\gamma^2+\Omega^2)^2}+\frac{mL^2\Omega^2}{32\omega_0\tau W}\frac{(\gamma^2+\Omega^2)^2}{2\gamma_1\sin^2\Psi[(\gamma-\gamma_1)^2+\Omega^2]}+\cot\Psi.\tag{21}$$

This value characterizes the scheme sensitivity. Our goal is to have this value as small as possible. In the next subsection we will perform two possible optimizations of ξ^2, in narrow and wide frequency bands.

C. Optimization of ξ^2

1. Narrowband optimization

Let optimize Eq. (21) at some fixed frequency. A possible situation when such optimization can be useful is the detection of gravitational radiation emitted by quasimonochromatic sources. Compact quickly rotating neutron stars, i.e., pulsars, may be an example of such sources. Gravitational radiation from pulsars is quasimonochromatic and relatively weak so it is crucial to have high sensitivity in a narrow frequency band to detect these sources. So it is convenient to find the minimum of ξ^2 at the source main frequency Ω_0. If we suppose that optical losses are small enough, i.e., $\alpha\ll\Omega_0$, then the minimal value of ξ will be equal to

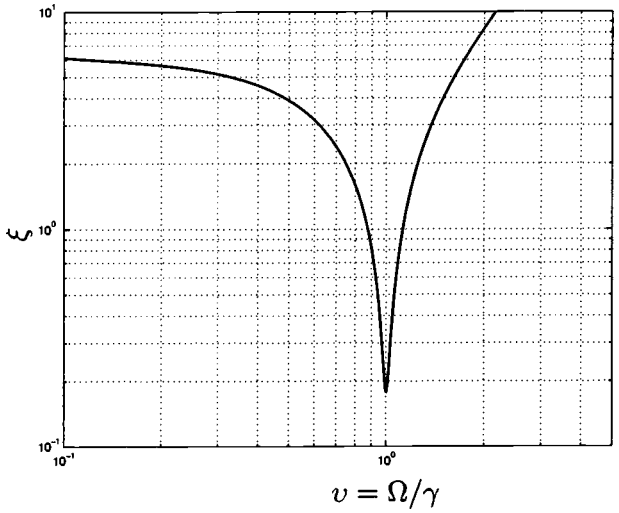

FIG. 6. Plot of $\xi=\sqrt{S_{SM}/S_{SQL}}$, optimized at some fixed frequency Ω_0. For given $\Omega_0=10^3$ s^{-1} and fixed optical loss contribution to the total half bandwidth $\alpha=1$ s^{-1} (see Table II), one should take the following parameters to obtain the best sensitivity at given frequency: total half bandwidth $\gamma=\Omega_0$, circulating power $W=(mL^2\Omega_0^3/8\omega_0\tau)\sqrt{\Omega_0/\alpha}\simeq 27$ MW, and $\cot\Psi=-\sqrt{\Omega_0/\alpha}\simeq -3\times10^{-2}$. The minimal ξ in that case will be equal to $\sqrt[4]{\alpha/\Omega_0}\simeq 0.18$.

$$\xi_{min}=\sqrt[4]{\varepsilon}=\sqrt[4]{\frac{\alpha}{\Omega_0}}, \tag{22}$$

and is reached at $\gamma_{opt}=\Omega_0$, optical circulating power $W_{opt}=(mL^2\Omega_0^3/8\omega_0\tau)\sqrt{\Omega_0/\alpha}$, and homodyne angle defined by the formula $\cot\Psi_{opt}=-\sqrt{\Omega_0/\alpha}$ (see Appendix D for details). For $\alpha=1$ s^{-1} it will be equal to $\xi\simeq 0.18$. For the LIGO interferometer the optical power necessary to reach the above value of ξ is equal to $W_{opt}\simeq 27$ MW.

Unfortunately, at frequencies different from Ω_0 the value of ξ is much worse. The behavior of the function ξ at different frequencies is presented in Fig. 6. We can see that significant gain in sensitivity compared to the SQL can be achieved in a very narrow frequency band of about several tens of hertz. Thus, this regime of the speed meter operation, which we prefer to call the ''narrowband'' regime, can be used to beat the SQL by a significant amount only in a narrowband near some arbitrarily chosen frequency for the purposes of weak quasimonochromatic sources detection.

2. Wideband optimization

Contrary to the narrowband case considered above, the vast majority of gravitational-wave sources either radiate in a relatively wide frequency band, or their main frequency is unknown. In both cases it is necessary to perform a wideband detection procedure. This problem cannot be solved as easily as the previous one, because there are no criteria for what should be the frequency bandwidth value and what sensitivity should be reached within the ranges of this band. As there is no clarity on this question it seems convenient to represent the variety of different possible regimes of operation that the speed meter is capable of. Therefore we will suppose that the optical power W circulating in the arms of the interferometer and the resonator halfbandwidth γ are fixed. Then by varying the homodyne angle Ψ it is possible to obtain a variety of different sensitivity curves. These curves for three different values of the circulating optical power $W=1$, 3, and 10 MW are presented by thin curves in Figs. 7, 8, and 9, respectively. By varying the homodyne angle it is possible to reach a sensitivity even three times better than SQL in a relatively wide frequency band. It is also possible to choose the frequency where the best sensitivity is reached by changing the homodyne angle, i.e., an increase of Ψ leads to a sensitivity curve offset into the lower frequency domain. It should also be noted that the increase of circulating power in this regime leads to a reduc-

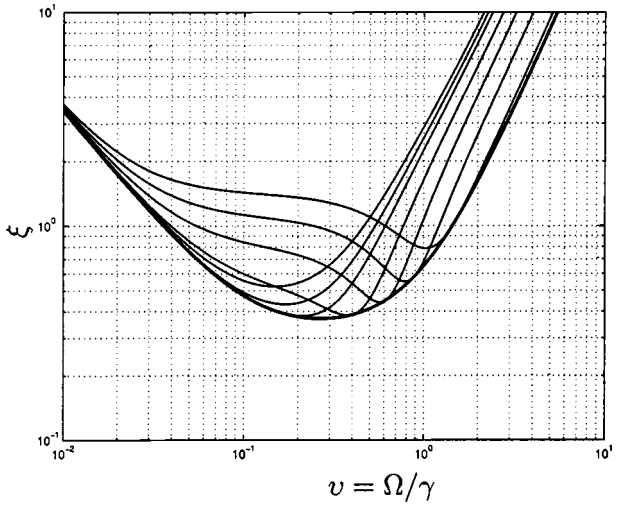

FIG. 7. Plots of ξ for circulating optical power $W=1$ MW and several fixed homodyne angles (thin curves; the curve with rightmost minimum corresponds to the least angle). Bold black curve corresponds to frequency-dependent homodyne angle.

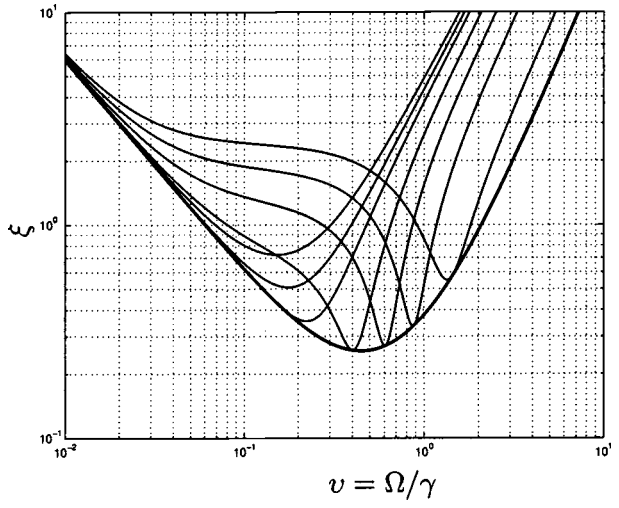

FIG. 8. Plots of ξ for circulating optical power $W=3$ MW and several fixed homodyne angles (thin curves; the curve with rightmost minimum corresponds to the least angle). Bold black curve corresponds to frequency-dependent homodyne angle.

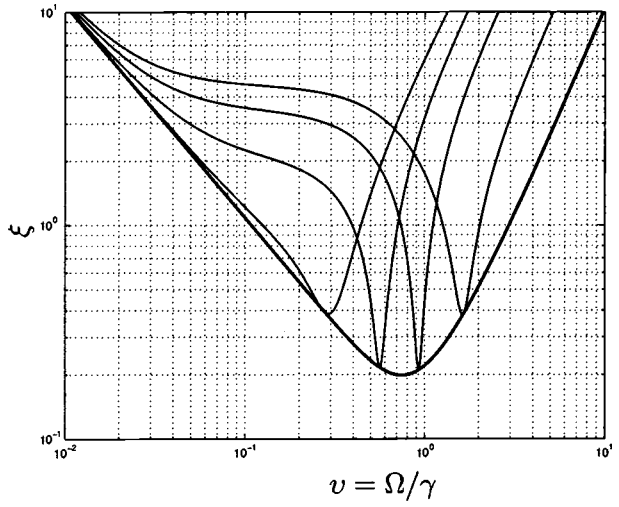

FIG. 9. Plots of ξ for circulating optical power $W=10$ MW and several fixed homodyne angles (thin curves; the curve with rightmost minimum corresponds to the least angle). Bold black curve corresponds to frequency-dependent homodyne angle.

tion of the frequency band where ξ is less than 1; therefore it is reasonable to use moderate values of the optical powers.

Using the technique of frequency-dependent variational readout suggested in [24], it is possible to increase the sensitivity of the speed meter significantly in a wide frequency band. The achievable sensitivities in this case are represented in the same figures by bold black curves. Here is the dependence of $\Psi(\Omega)$ that allows us to obtain the above mentioned results:

$$\Psi(\Omega)=\pi-\arctan\left(\frac{mL^2}{32\omega_0\tau W}\cdot\frac{\Omega^2(\gamma^2+\Omega^2)^2}{\gamma_1(\alpha^2+\Omega^2)}\right). \quad (23)$$

D. Delay line and ring cavity vs Fabry-Pérot in speed meter topology

It seems resonable to discuss some issues concerning the performance of the analyzed scheme and the schemes of speed meter interferometers proposed in [12], that are based on using delay lines (DLs) and ring cavities (RCs) instead of FP cavities. In the lossless limit all the above mentioned schemes provide practically the same sensitivity and there are no significant differences in their performance. When taking internal optical losses in cavity elements into account, one can readily realize that the RC interferometer will have approximately a 1.5 times higher loss coefficient α compared to the FP interferometer, as the ring cavity requires three mirrors instead of two. A simple evaluation can show that in the narrowband regime the RC speed meter will require $\sqrt{1.5}\simeq 1.22$ times more optical power to achieve the best sensitivity, which is $\sqrt[4]{1.5}\simeq 1.11$ (22) times worse than the FP speed meter. The wideband regime is less susceptible to an increase of α, but it can slightly decrease the frequency band where the speed meter sensitivity is better than the SQL. Another point that, in our opinion, should be taken into account is that ring cavity design requires placing two large mirrors close to each other. It might be difficult to find an additional place for one more mirror in existing interferometer facilities.

On the other hand, the RC interferometer has an important advantage. It does not require such devices as a polarization beam splitter and quarter-wave plates to be used, and can be constructed using only traditional optical elements, whose properties are well studied.

As for delay lines, they will provide practically the same sensitivity as FP cavities even taking optical losses into account. Nevertheless, in large scale interferometers it is quite difficult, in our opinion, to implement delay lines, as it requires larger mirrors compared to FP cavities in order to provide a necessary number of light beam round trips. Moreover, the delay line, we suppose, should be very sensitive to mirror tilts, which is quite crucial for kilometer-long cavities. Therefore, it seems impractical to use delay lines in large scale interferometers, while it can be a good candidate for shorter QND interferometers.

V. CONCLUSION

In this section we will sum up the results of our consideration. The following conclusions can be made.

The attempts to increase speed meter sensitivity by introducing a signal-recycling mirror or replacing arm cavities by this mirror will not be successful, because unlike the position meter, the speed meter sensitivity depends nonsymmetrically upon the transmittances of the arm cavity input mirrors and SRM. The influence of the ITM is considerably greater than the SRM influence because in the speed meter the light beam passes consequently through both cavities before it is reflected from the SRM. Therefore, it is convenient to use arm cavities in gravitational-wave detectors based on the speed meter principle.

The speed meter topology of gravitational-wave antennas allows one to achieve a sensitivity about three times better than the SQL in a relatively wide frequency band, preserving the optical power circulating in the arms at a reasonable level of 1 MW. Moreover, its sensitivity can be improved and its frequency band can be significantly increased if one applies a variational readout technique.

The ultimate sensitivity a speed meter is capable of is defined by two factors, the optical losses and bandwidths of arm cavities and, therefore, the circulating power. This sensitivity can be expressed in terms of these factors as

$$\xi=\frac{h}{h_{SQL}}=\sqrt[4]{\frac{\alpha}{\gamma}},$$

where h is the metric variation which can be measured by the speed meter, h_{SQL} is the standard quantum limit for h, and α is the optical loss contribution to the total interferometer halfbandwidth γ. However, a high sensitivity (small ξ) requires a large amount of circulating optical power (about tens of megawatts) and can be achieved in a relatively narrow frequency band. In our opinion, the best operation mode for the speed meter is the wideband regime with frequency-dependent readout.

ACKNOWLEDGMENTS

The author would like to express his sincere gratitude to Professor F. Ya. Khalili for the interesting subject of investigation and help and advice. The author also would like to thank V. B. Braginsky, S. P. Vyatchanin, and S. E. Strigin for helpful discussions and encouragement. Special thanks go to K. Danzmann, R. Schnabel, and all members of the GEO600 team for fruitful talks, valuable conversations, and hospitality. This paper is supported in part by NSF and Caltech Grant No. PHY0098715, by the Russian Foundation for Basic Research, and by the Russian Ministry of Industry and Science.

APPENDIX A: DERIVATION OF SPECTRAL DENSITIES FOR SIMPLE CASE

1. Input-output relation derivation

Here we will obtain the formulas for the quantum noise spectral densities, presented in Sec. II by the expressions (4). The input light can be described by the formula (1). The input amplitudes are the following (the subscripts *w*,*e*,*s*,*n* are for light beams corresponding to that part of the scheme; for example, A_w means the classical amplitude of a light beam propagating in the western direction):

$$A_w = A, \quad A_s = 0, \tag{A1}$$

and the corresponding sideband operators are

$$\hat{a}_w, \quad \hat{a}_s. \tag{A2}$$

As we mentioned above we are able to introduce additional pumping through the central mirror. This additional pumping increases the light power in the scheme and does not create additional noise; therefore, it increases the scheme sensitivity. To describe it we will introduce the complex parameter $\eta = \eta e^{i\Phi} = \sqrt{2}C/A$ which is equal to the ratio of the light amplitude at the end mirrors with additional pumping ($C = A/\sqrt{2} + A_{add}$) and the light amplitude after the beam splitter ($A/\sqrt{2}$) (which is equal to the amplitude at the end mirror provided that the central mirror is ideally reflecting, i.e., in the lossless case).

Taking all the above into account one can easily obtain that the classical output of the scheme is equal to

$$B_s = 0, \tag{A3}$$

and the corresponding sideband output is equal to

$$\begin{aligned}\hat{b}_s(\omega) &= ir\hat{a}_s(\omega)e^{4i\omega\tau} - i\alpha\frac{-\hat{g}_n(\omega) + i\hat{g}_e(\omega)}{\sqrt{2}}e^{2i\omega\tau} \\ &\quad - 2\kappa(\omega)A(ire^{i(\omega_0+3\omega)\tau} - \eta e^{i(\omega_0+\omega)\tau})x_-(\omega_0-\omega) \\ &= \beta_{input}\hat{a}_s + \beta_{loss}\hat{g}_s + \mathcal{K}_{simple}x_-;\end{aligned} \tag{A4}$$

see Eq. (2) for notation.

2. Radiation pressure noise spectral density $S_F(\Omega)$

The radiation pressure force corresponding to system mode x_- is equal to

$$\begin{aligned}\hat{F} &= \hat{F}_e - \hat{F}_n \\ &= 2\hbar\int_0^\infty \kappa(\omega)A^*\Bigg[(ie^{i(\omega-\omega_0)\tau} + \eta e^{-i\Phi}re^{i(3\omega-\omega_0)\tau})\hat{a}_s(\omega) \\ &\quad - \sqrt{2}\alpha\eta e^{-i\Phi}e^{i(\omega-\omega_0)\tau}\frac{-\hat{g}_n(\omega) + i\hat{g}_e(\omega)}{\sqrt{2}}\Bigg]e^{i(\omega_0-\omega)t}\frac{d\omega}{2\pi} \\ &\quad + \text{H.c.},\end{aligned} \tag{A5}$$

where $\hat{F}_e$ and $\hat{F}_n$ are the radiation pressure fluctuational forces acting upon the eastern and northern movable mirrors, respectively.

In order to calculate the radiation pressure spectral density one should calculate the symmetric correlation function

$$B_F(t-t') = \frac{1}{2}\langle 0|[\hat{F}(t)\hat{F}(t') + \hat{F}(t')\hat{F}(t)]|0\rangle, \tag{A6}$$

where $|0\rangle$ is the radiation field ground state. If we calculate this value we obtain

$$\begin{aligned}B_F(t-t') = \frac{1}{2}\Bigg\{&\int_0^\infty |F(\omega)|^2 e^{i(\omega_0-\omega)(t-t')}\frac{d\omega}{2\pi} \\ &+ \int_0^\infty |F(\omega)|^2 e^{-i(\omega_0-\omega)(t-t')}\frac{d\omega}{2\pi}\Bigg\},\end{aligned} \tag{A7}$$

where

$$\begin{aligned}|F(\omega)|^2 &= 4\hbar^2\kappa^2(\omega)|A|^2 \\ &\quad \times[|(e^{i(\omega-\omega_0)\tau} - i\eta e^{i\Phi}re^{i(3\omega-\omega_0)\tau})|^2 + \alpha^2\eta^2].\end{aligned}$$

In order to obtain this result one should take into account that $\langle 0|\hat{a}(\omega)\hat{a}^\dagger(\omega')|0\rangle = 2\pi\delta(\omega-\omega')$. The radiation pressure spectral density can be defined as

$$\begin{aligned}S_F(\Omega) &= \int_{-\infty}^\infty B_F(t)e^{-i\Omega t}dt = \frac{1}{2}[S'(\Omega) + S'(-\Omega)] \\ &= \frac{16\hbar\omega_0 W}{c^2}\cdot\frac{1/2 + \eta^2/2 - \eta r\sin\Phi\cos 2\Omega\tau}{1+\eta^2}.\end{aligned} \tag{A8}$$

In order to provide the speed meter mode of operation we need to set $\Phi = \pi/2$; then one will obtain that

$$S_F(\Omega) = \frac{8\hbar\omega_0 W}{c^2}\cdot\frac{1+\eta^2 - 2\eta r\cos(2\Omega\tau)}{1+\eta^2}. \tag{A9}$$

3. Shot noise spectral density $S_x(\Omega)$

The output signal of the scheme is mixed up with the local oscillator wave in order to detect the phase shift due to the end mirror displacement in the optimal way. This mixed radiation enters the homodyne detector. The photocurrent of the detector is proportional to the following time-averaged value:

$$\begin{aligned}\hat{I}_{p.d.}(t) &\sim \overline{2E_{b_s}(t)\cos(\omega_0 t+\phi_{LO})} \\ &= \int_0^\infty \sqrt{\omega}\hat{b}_s(\omega)e^{i(\omega_0-\omega)t+i\phi_{LO}}\frac{d\omega}{2\pi}+\text{H.c.} \\ &= \int_{-\infty}^{\infty} K(\Omega)[\hat{x}_{fluct}(\Omega)+x_-(\Omega)]e^{i\Omega t}\frac{d\Omega}{2\pi},\end{aligned} \tag{A10}$$

where ϕ_{LO} is the local oscillator phase, $\hat{r}(\Omega)$ is the noise operator whose spectral density is equal to unity, and $K(\Omega)$ is equal to

$$K(\Omega)=-\frac{4\omega_0^{3/2}|A|}{c}e^{-3i\Omega\tau}[r\sin\Psi+\eta e^{2i\Omega\tau}\cos(\Phi+\Psi)], \tag{A11}$$

where $\Psi=\phi_{LO}+\arg A$. The fluctuations of the coordinate are described by the operator

$$\hat{x}_{fluct}(\Omega)=\frac{\hat{r}(\Omega)}{K(\Omega)}. \tag{A12}$$

Finally, assuming $\Phi=\pi/2$, the coordinate noise spectral density is equal to

$$S_x(\Omega)=\frac{\hbar c^2}{32\omega_0 W\sin^2\Psi}\cdot\frac{1+\eta^2}{r^2+\eta^2-2r\eta\cos(2\Omega\tau)}. \tag{A13}$$

4. Cross-correlation spectral density $S_{xF}(\Omega)$

Now we know everything needed to calculate the cross-correlation spectral density $S_{xF}(\Omega)$. In order to do this one should find the cross-correlation function of Eq. (A5) and $\hat{x}_{fluct}(\Omega)$. Using the same algorithm as in previous subsections one obtains that

$$S_{xF}(\Omega)=-\frac{\hbar}{2}\cot\Psi. \tag{A14}$$

APPENDIX B: POWER- AND SIGNAL-RECYCLED SPEED METER INTERFEROMETER SENSITIVITY: PRECISE ANALYSIS

1. Input-output relations for power- and signal-recycled speed meter interferometer

In this appendix we will analyze the scheme of a speed meter interferometer with power (PRM) and signal (SRM) recycling mirrors installed (see Fig. 10). Here we will confirm by exact calculations the results of the qualitative consideration presented in Sec. III.

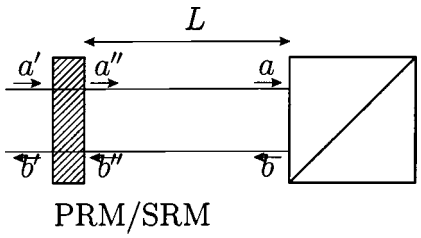

FIG. 10. Power- and signal-recycled speed meter interferometer.

Let consider the influence of additional optical elements on the input-output relations.

Figure 11 represents the situation common for PRM and SRM. Beams a and b represent light entering and leaving the beam splitter, and beams a' and b' stand for light entering and leaving the PRM/SRM. The length L of the recycling cavity should be chosen in the way that provides the maximal values of circulating power in the case of the PRM, and signal sidebands in the case of the SRM.

a. Power recycling mirror

Power recycling influences the value of the circulating power only, as quantum fluctuations from the laser that are influenced by the PRM return back to the laser due to dark port tuning of the interferometer, and do not contribute to the output signal. The interferometer circulating power depends upon the quadrature amplitude A of the beam a as

$$W=\hbar\omega_0|A|^2.$$

Then we need to express A in terms of A', the amplitude of the beam a' entering the PRM. One can write down the following equations:

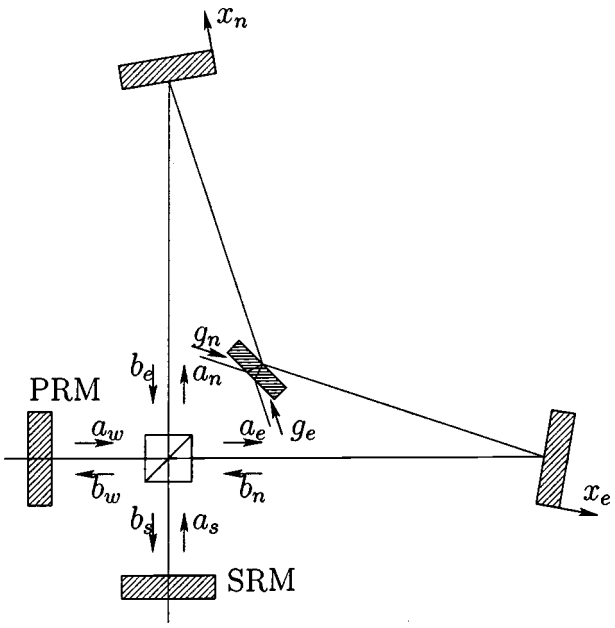

FIG. 11. Power recycling/signal recycling mirrors.

$$A''=it_{PR}A'-r_{PR}B'', \quad A''=Ae^{-i\phi_{PR}}, \tag{B1a}$$

$$B'=it_{PR}B''-r_{PR}A'', \quad B''=Be^{i\phi_{PR}}, \tag{B1b}$$

$$B=i(1-\alpha_{loss})A, \tag{B1c}$$

where t_{PR} and r_{PR} are the PRM transmittance and reflectivity, $\phi_{PR}=\omega_0 L/c$, and α_{loss} represents losses in the entire scheme (we will neglect these losses in this calculation as α_{loss} is sufficiently small). Solving these equations leads to the following expression:

$$A=\frac{it_{PR}e^{i\phi_{PR}}}{1+ir_{PR}e^{2i\phi_{PR}}}A'. \tag{B2}$$

In order to maximize the circulating power one should tune the PR cavity so that $\phi_{PR}=\pi/4$; then we obtain that

$$W_{PR}=\frac{t_{PR}^2 W_0}{(1-r_{PR})^2}\simeq\frac{4W_0}{t_{PR}^2}, \tag{B3}$$

where $W_0=\hbar\omega_0|A'|$, and $W_{PR}=\hbar\omega_0|A|^2$.

b. Signal recycling mirror

In the case of the signal-recycling cavity only the quantum fluctuation transformation is worth examining. As the interferometer is tuned so that the output port is kept "dark," the classical amplitude of the beam leaving the BS is equal to zero. Now a and b stand for the fluctuations entering and leaving the BS, while a' and b' stand for fluctuations entering and leaving the SRM. Therefore we write down the following equations:

$$\hat{b}'=it_{SR}e^{i\phi_{SR}}\hat{b}-r_{SR}\hat{a}', \quad \hat{a}'e^{-i\phi_{SR}}=it_{SR}\hat{a}'-r_{SR}e^{i\phi_{SR}}\hat{b}, \tag{B4}$$

where t_{SR} and r_{SR} are the SRM transmittance and reflectivity, and $\phi_{SR}=\omega_0 L/c$. In these equations we should suppose $\hat{a}'\equiv\hat{a}_s$, $\hat{b}'\equiv\hat{b}_s$, and the equation that gives the relation between these operators is represented by the expression (2).

The solution of these equations gives us the following expression for the PR and SR speed meter output signal:

$$\hat{b}_s'=-\left(r_{SR}+\frac{t_{SR}^2 e^{2i\phi_{SR}}\beta_{input}}{1+r_{SR}\beta_{input}e^{2i\phi_{SR}}}\right)\hat{a}_s' + \frac{it_{SR}e^{i\phi_{SR}}\beta_{loss}}{1+r_{SR}\beta_{input}e^{2i\phi_{SR}}}\hat{g}_s+\mathcal{K}_{SR}x_-, \tag{B5}$$

where

$$\mathcal{K}_{SR}=\frac{it_{SR}e^{i\phi_{SR}}\beta_{loss}}{1+r_{SR}\beta_{input}e^{2i\phi_{SR}}}\mathcal{K}_{simple},$$

and β_{input}, β_{loss}, and $\mathcal{K}_{simple}$ are defined in Eq. (2). The value of ϕ_{SR} is chosen so that the output signal is maximal, i.e., $\mathcal{K}_{SR}\to\max$. Therefore, the signal-recycling cavity should be tuned in a way to provide $\phi_{SR}=\pi/4$.

Now we are able to calculate the spectral densities of radiation pressure and shot noise and their cross-correlation spectral density.

2. Radiation pressure noise spectral density $S_F(\Omega)$

In order to calculate the radiation pressure noise spectral density for a power- and signal-recycled speed meter interferometer one needs to replace operator $\hat{a}_s$ in formula (A5) of the previous appendix by the operator $\hat{a}_s'$ that can be expressed in terms of $\hat{a}_s$ and $\hat{g}_s$ as

$$\hat{a}_s'=\frac{it_{SR}e^{i\phi_{SR}}\hat{a}_s-r_{SR}\beta_{loss}e^{2i\phi_{SR}}\hat{g}_s-r_{SR}e^{2i\phi_{SR}}\mathcal{K}_{simple}x_-}{1+r_{SR}\beta_{input}e^{2i\phi_{SR}}}. \tag{B6}$$

After the same operations as in Appendix one obtains that the radiation pressure noise spectral density in the case of a power- and signal-recycled speed meter interferometer is equal to

$$S_F(\Omega)=\frac{16\hbar\omega_0\tau W_{PR}}{c^2}\cdot\frac{(\gamma+\gamma_{SR})(\gamma\gamma_{SR}+\Omega^2)}{(\gamma+\gamma_{SR})^2+4\Omega^2}. \tag{B7}$$

3. Shot noise spectral density $S_x(\Omega)$

To obtain the expression for the shot noise spectral density in the case of a signal-recycled interferometer we should use the same procedure as in Appendix but for one exception. We should substitute the value of $\mathcal{K}_{simple}$ by $\mathcal{K}_{SR}$. To account for power recycling we should also write down W_{PR} instead of W. Finally we obtain the following formula:

$$S_x(\Omega)=\frac{\hbar c^2}{64\omega_0\tau W_{PR}\sin^2\Psi}\cdot\frac{(\gamma+\gamma_{SR})^2+4\Omega^2}{\gamma_{SR}(\gamma^2+\Omega^2)}. \tag{B8}$$

4. Cross-correlation spectral density $S_{xF}(\Omega)$

The cross-correlation spectral density in this case is the same as in the previous section and is common for all interferometric schemes considered with homodyne detection:

$$S_{xF}(\Omega)=-\frac{\hbar}{2}\cot\Psi. \tag{B9}$$

5. Power- and signal-recycled speed meter sensitivity

The total noise of the PR and SR speed meter is described by the same formula as Eq. (3). The spectral densities of noises in this particular case can be obtained from the formulas (B7), (B8), and (B9).

Being substituted in Eq. (3) and divided by $S_{SQL}=\hbar m\Omega^2$, these formulas will give us the expression for the factor ξ^2 by which one can beat the SQL using the PR and SR speed meter:

$$\xi^2 = P_{SR}\frac{(\gamma_{SR}+\gamma)(\gamma\gamma_{SR}+\Omega^2)}{\Omega^2[(\gamma+\gamma_{SR})^2+4\Omega^2]} + \frac{1+\cot^2\Psi}{4P_{SR}}\cdot\frac{\Omega^2[(\gamma+\gamma_{SR})^2+4\Omega^2]}{\gamma_{SR}(\gamma^2+\Omega^2)} + \cot\Psi, \tag{B10}$$

where $P_{SR}=16\omega_0\tau W_{PR}/mc^2$, $\gamma=(1-r)/2\tau$ is the interferometer half bandwidth part due to optical losses, and $\gamma_{SR}=(1-r_{SR})/2\tau$ is the part of the half bandwidth due to the signal-recycling mirror. We can now optimize this expression at some fixed frequency Ω_0 with respect to the homodyne angle Ψ and circulating power W_{PR}. The optimal circulating power W_{opt} and homodyne angle Ψ_{opt} for the considered scheme are equal to

$$W_{opt}\simeq\frac{mc^2}{32\omega_0\tau}\left(1+4\frac{\Omega_0^2}{\gamma_{SR}^2}\right)\sqrt{\frac{\Omega_0^2}{\gamma\gamma_{SR}}},$$

$$\Psi_{opt}\simeq-\arctan\sqrt{\frac{\gamma\gamma_{SR}}{\Omega_0^2}}, \tag{B11}$$

and the minimal value of ξ that can be achieved at frequency Ω_0 is

$$\xi_{opt}\simeq\sqrt[4]{\frac{\gamma\gamma_{SR}}{\Omega_0^2}}. \tag{B12}$$

We can see that to beat the SQL considerably using a signal-recycled speed meter one needs to decrease internal losses. Decreasing γ_{SR} (or increasing r_{SR}) will also increase the scheme sensitivity at a given frequency but at the sacrifice of sensitivity at other frequencies.

Let us estimate the optimal circulating power that is necessary to obtain $\xi\simeq0.1$. Let us substitute the following parameters:

$$\Omega_0=10^3\ \mathrm{s}^{-1},\ m=5\ \mathrm{kg},\ L=600\ \mathrm{m},$$
$$\omega_0=1.77\times10^{15}\ \mathrm{s}^{-1},$$
$$1-r=10^{-5}, \tag{B13}$$

that are typical for the GEO 600 interferometer. To obtain $\xi_{opt}=0.1$ one needs $\gamma_{SR}=40\ \mathrm{s}^{-1}$ $(1-r_{SR}=1.6\times10^{-4})$ and circulating power of the order of

$$W_{opt}=10^{11}\ \mathrm{W}. \tag{B14}$$

We can see that the considered scheme of a power- and signal-recycled speed meter can hardly be implemented in gravitational-wave detection, as it requires an enormous amount of optical power and its sensitivity is high only in a very narrow frequency band.

This result confirms the statement we made in Sec. III, i.e., in order to achieve the same sensitivity as a position meter with Fabry-Pérot cavities in the arms, the speed meter requires a highly reflecting SRM to be used and therefore an enormous amount of pumping power is needed. Taking this into account it is reasonable to conclude that the scheme with Fabry-Pérot cavities in both arms without a SRM looks like the best candidate for implementing a speed meter interferometer.

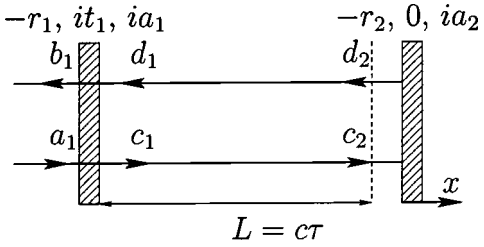

FIG. 12. Fabry-Pérot cavity with movable mirror.

APPENDIX C: DERIVATION OF SPECTRAL DENSITIES FOR SPEED METER INTERFEROMETER WITH FABRY-PÉROT CAVITIES IN ARMS

1. Fabry-Pérot input-output relations

To obtain input-output (IO) relations for the scheme presented in Fig. 5 one needs to know the IO relations for a Fabry-Pérot cavity with movable end mirror. The case of two movable mirrors will give the same result but when investigating cavity dynamics one should replace the end mirror displacement x by the difference x_1-x_2 of each mirror displacement, and the mirror masses should be taken at one-half of the real value to account for changes in radiation pressure forces.

Consider the FP cavity presented in Fig. 12. We suppose the end mirror to have zero transmittance for the same reason as in Sec. IV A.

Suppose we know the classical amplitude of the internal field C_1 and input quantum fluctuations $\hat{a}_1$ of the input light. To obtain expressions for the internal and output fields one needs to solve the following equations:

$$\hat{b}_1(\omega)=-r_1\hat{a}_1(\omega)+it_1\hat{c}_1(\omega)+ia_1\hat{g}_{12}(\omega),$$

$$\hat{d}_1(\omega)=it_1\hat{a}_1(\omega)-r_1\hat{c}_1(\omega)+ia_1\hat{g}_{11}(\omega),$$

$$\hat{d}_2(\omega)=-r_2\hat{c}_2(\omega)+ia_2\hat{g}_{21}(\omega)-2i\kappa(\omega)r_2C_2x(\omega_0-\omega),$$

$$\hat{c}_2(\omega)=\hat{d}_1(\omega)e^{i\omega\tau},\quad \hat{d}_2(\omega)=\hat{c}_1(\omega)e^{-i\omega\tau}. \tag{C1}$$

The solution can be written as

$$\hat{b}_1=\frac{1}{\mathcal{L}(\omega)}[\mathcal{B}(\omega)\hat{a}_1(\omega)-e^{2i\omega\tau}r_2t_1a_1\hat{g}_{11}(\omega) + ia_1\mathcal{L}(\omega)\hat{g}_{12}(\omega)+e^{i\omega\tau}t_1a_2\hat{g}_{21}(\omega) - 2\kappa(\omega)e^{i\omega\tau}r_2t_1C_2x(\omega_0-\omega)], \tag{C2a}$$

$$\hat{c}_2=\frac{1}{\mathcal{L}(\omega)}[-ie^{i\omega\tau}t_1\hat{a}_1(\omega)-ie^{i\omega\tau}a_1\hat{g}_{11}(\omega)$$
$$+ie^{2i\omega\tau}r_1a_2\hat{g}_{21}(\omega)-2i\kappa(\omega)e^{2i\omega\tau}r_1r_2C_2x(\omega_0-\omega)], \tag{C2b}$$

$$\hat{d}_2=\frac{1}{\mathcal{L}(\omega)}[ie^{i\omega\tau}t_1r_2\hat{a}_1(\omega)+ie^{i\omega\tau}r_2a_1\hat{g}_{11}(\omega)-ia_2\hat{g}_{21}(\omega)$$
$$+2i\kappa(\omega)r_2C_2x(\omega_0-\omega)], \tag{C2c}$$

where

$$\mathcal{L}(\omega)=r_1r_2e^{2i\omega\tau}-1, \quad \mathcal{B}(\omega)=r_1-e^{2i\omega\tau}r_2(r_1^2+t_1^2). \tag{C3}$$

The expressions (C2) represent the FP cavity input-output relations.

2. Radiation pressure noise in FP cavity

In this subsection we will obtain the expression for the radiation pressure force acting upon the movable mirror of the FP cavity. In accordance with the formula for the radiation pressure we can write down the following:

$$\hat{F}_{rp}=\frac{\hat{W}_{c_2}+\hat{W}_{d_2}}{c}=\frac{\overline{\hat{E}_{c_2}^2}+\overline{\hat{E}_{d_2}^2}}{4\pi}\mathcal{A}. \tag{C4}$$

Taking into account the expressions (C2) one can obtain

$$\hat{F}(t)=F_0+\hbar\int_0^\infty\kappa(\omega)[C_2^*\hat{c}_2(\omega)+D_2^*\hat{d}_2(\omega)]$$
$$\times e^{i(\omega_0-\omega)t}\frac{d\omega}{2\pi}+\text{H.c.}$$
$$=F_0+\hbar\int_0^\infty\kappa(\omega)[F_{a_1}\hat{a}_1(\omega)+F_{g_{11}}\hat{g}_{11}(\omega)$$
$$+F_{g_{21}}\hat{g}_{21}(\omega)]e^{i(\omega_0-\omega)t}\frac{d\omega}{2\pi}+\text{H.c.}, \tag{C5}$$

where

$$F_{a_1}\simeq-\frac{2it_1e^{i\omega\tau}C_2^*}{\mathcal{L}(\omega)}, \quad F_{g_{11}}\simeq-\frac{2ia_1e^{i\omega\tau}C_2^*}{\mathcal{L}(\omega)},$$
$$F_{g_{21}}\simeq\frac{ia_2(e^{2i\omega\tau}+1)C_2^*}{\mathcal{L}(\omega)}, \tag{C6}$$

and $F_0=\hbar\omega_0|C_2|^2(1+r_2^2)/c\simeq 2\hbar\omega_0|C_2|^2/c$ is the constant classical radiation pressure force. Items that correspond to other noise operators are neglected as they are small compared to the above values.

3. Input-output relation derivation

Now we can write down the IO relations for our speed meter scheme. One can note that the light beam between input and output moments is sequentially reflected from two FP cavities. Therefore, the sideband operator that describes the output beam for the first cavity at the same time describes the input beam for the second one. Moreover, the beam that enters the cavity for the first time and the beam that enters the cavity after being reflected once do not interact as they have different polarizations (↻ and ↺ in our case). Then, the beams that leave the scheme falling to the beam splitter from the north and east are characterized by sideband operators $\hat{c}_n$ and $\hat{c}_e$ that can be expressed in terms of input beam operators as

$$\hat{c}_n=\frac{1}{\mathcal{L}(\omega)}[\mathcal{B}(\omega)\hat{b}_n^I(\omega)-e^{2i\omega\tau}r_2t_1a_1\hat{g}_{e_{11}}^{II}(\omega)$$
$$+e^{i\omega\tau}t_1a_2\hat{g}_{e_{21}}^{II}(\omega)+i\sqrt{2}\kappa(\omega)e^{i\omega\tau}r_2t_1Fx_e(\omega_0-\omega)], \tag{C7a}$$

$$\hat{c}_e=\frac{1}{\mathcal{L}(\omega)}[\mathcal{B}(\omega)\hat{b}_e^I(\omega)-e^{2i\omega\tau}r_2t_1a_1\hat{g}_{n_{11}}^{II}(\omega)$$
$$+e^{i\omega\tau}t_1a_2\hat{g}_{n_{21}}^{II}(\omega)-\sqrt{2}\kappa(\omega)e^{i\omega\tau}r_2t_1Fx_n(\omega_0-\omega)], \tag{C7b}$$

where F is the amplitude inside the cavity during the second reflection, $\hat{b}_{1_n}^I$ and $\hat{b}_{1_e}^I$ are defined by formula (C2a) by replacing the index 1 by $^I_{1_n}$ and $^I_{1_e}$ (the superscript I means the first reflection and the superscript II means the second reflection from the FP cavity), and C_2 by $E_n=iE/\sqrt{2}$ and $E_e=-E/\sqrt{2}$, where E is the amplitude inside the cavity during the first reflection. Here we also introduced additional pumping to compensate the energy losses due to absorption in the FP cavities. We suppose that this pumping should feed the main beam before it enters the second cavity; then the parameter $\boldsymbol{\eta}=F_e/E_e=F_n/E_n$. Now we are able to calculate the output beam sideband operator $\hat{c}_s=(i\hat{c}_n-\hat{c}_e)/\sqrt{2}$:

$$\hat{c}_s=\frac{1}{\mathcal{L}^2(\omega)}\{i\mathcal{B}^2(\omega)\hat{a}_s^I(\omega)$$
$$+i\mathcal{B}(\omega)[e^{2i\omega\tau}r_2t_1a_1\hat{g}_{s_{11}}^I(\omega)-e^{i\omega\tau}t_1a_2\hat{g}_{s_{21}}^I(\omega)]$$
$$-i\mathcal{L}(\omega)[e^{2i\omega\tau}r_2t_1a_1\hat{g}_{w_{11}}^{II}(\omega)-e^{i\omega\tau}t_1a_2\hat{g}_{w_{21}}^{II}(\omega)]$$
$$-[\mathcal{B}_1(\omega)-\boldsymbol{\eta}\mathcal{L}(\omega)]E\kappa(\omega)e^{i\omega\tau}r_2t_1x_-(\omega_0-\omega)\}, \tag{C8}$$

where $x_-=(x_n-x_e)/2$, $\hat{\alpha}_s=-(\hat{\alpha}_n+i\hat{\alpha}_e)/\sqrt{2}$, and $\hat{\alpha}_w=-(\hat{\alpha}_e+i\hat{\alpha}_n/\sqrt{2})$ (here $\hat{\alpha}$ stands for any bosonic operator).

4. Radiation pressure noise spectral density $S_F(\Omega)$

In order to calculate the radiation pressure noise for the speed meter as a whole we need to use the expression for radiation pressure fluctuational force acting upon the end

mirror of the Fabry–Pérot cavity, presented in Sec. C 2 by formula (C5). As in the simple scheme one can present the fluctuational force acting upon each of the FP cavity end mirrors as a sum of two independent items:

$$\hat{F}_e=\hat{F}_e^{\circlearrowleft}+\hat{F}_e^{\circlearrowright} \quad \text{and} \quad \hat{F}_n=\hat{F}_n^{\circlearrowleft}+\hat{F}_n^{\circlearrowright}, \tag{C9}$$

and the net force acting upon the scheme can be presented as

$$\hat{F}=\hat{F}^{\circlearrowleft}+\hat{F}^{\circlearrowright}, \tag{C10}$$

where

$$\hat{F}^{\circlearrowleft}=\hat{F}_n^{\circlearrowleft}-\hat{F}_e^{\circlearrowleft}$$

and

$$\hat{F}^{\circlearrowright}=\hat{F}_n^{\circlearrowright}-\hat{F}_e^{\circlearrowright}. \tag{C11}$$

Let us write down the explicit form of these expressions:

$$\hat{F}^{\circlearrowleft}(t)=F_0^{\circlearrowleft}+2\hbar\int_0^{\infty}\kappa(\omega)[F_{a_s}^{\circlearrowleft}\hat{a}_s(\omega)+F_{g_{s_{11}}}^{\circlearrowleft,I}\hat{g}_{s_{11}}^{I}(\omega)+F_{g_{s_{21}}}^{\circlearrowleft,I}\hat{g}_{s_{21}}^{I}(\omega)]e^{i(\omega_0-\omega)t}\frac{d\omega}{2\pi}+\text{H.c.}, \tag{C12a}$$

where $F_0^{\circlearrowleft}\simeq\hbar\omega_0|E|^2/c$ is the corresponding classical radiation pressure force,

$$F_{a_s}^{\circlearrowleft}\simeq\frac{2t_1e^{i\omega\tau}E^*}{\mathcal{L}(\omega)}, \tag{C12b}$$

$$F_{g_{s_{11}}}^{\circlearrowleft,I}\simeq\frac{2a_1e^{i\omega\tau}E^*}{\mathcal{L}(\omega)},$$

$$F_{g_{s_{21}}}^{\circlearrowleft,I}\simeq-\frac{ia_2(e^{2i\omega\tau}+1)E^*}{\mathcal{L}(\omega)}, \tag{C12c}$$

and

$$\hat{F}^{\circlearrowright}(t)=F_0^{\circlearrowright}+2\hbar\int_0^{\infty}\kappa(\omega)[F_{a_s}^{\circlearrowright}\hat{a}_s(\omega)+F_{g_{s_{11}}}^{\circlearrowright,I}\hat{g}_{s_{11}}^{I}(\omega)+F_{g_{s_{21}}}^{\circlearrowright,I}\hat{g}_{s_{21}}^{I}(\omega)+F_{g_{s_{11}}}^{\circlearrowright,II}\hat{g}_{s_{11}}^{II}(\omega)+F_{g_{s_{21}}}^{\circlearrowright,II}\hat{g}_{s_{21}}^{II}(\omega)]e^{i(\omega_0-\omega)t}\frac{d\omega}{2\pi}+\text{H.c.}, \tag{C13a}$$

where $F_0^{\circlearrowright}\simeq\hbar\omega_0\eta^2|E|^2/c$ is the corresponding classical radiation pressure force,

$$F_{a_s}^{\circlearrowright}\simeq-\frac{2t_1e^{i\omega\tau}\boldsymbol{\eta}^*E^*}{\mathcal{L}(\omega)}\cdot\frac{\mathcal{B}(\omega)}{\mathcal{L}(\omega)}, \tag{C13b}$$

$$F_{g_{s_{11}}}^{\circlearrowright,I}\simeq\frac{2a_1e^{i\omega\tau}\boldsymbol{\eta}^*E^*}{\mathcal{L}(\omega)}\cdot\frac{t_1a_1e^{2i\omega\tau}}{\mathcal{L}(\omega)},$$

$$F_{g_{s_{21}}}^{\circlearrowright,I}\simeq\frac{ia_2(e^{2i\omega\tau}+1)\boldsymbol{\eta}^*E^*}{\mathcal{L}(\omega)}\cdot\frac{t_1a_2e^{i\omega\tau}}{\mathcal{L}(\omega)}, \tag{C13c}$$

$$F_{g_{s_{11}}}^{\circlearrowright,II}\simeq-\frac{2a_1e^{i\omega\tau}\boldsymbol{\eta}^*E^*}{\mathcal{L}(\omega)},$$

$$F_{g_{s_{21}}}^{\circlearrowright,II}\simeq-\frac{ia_2(e^{2i\omega\tau}+1)\boldsymbol{\eta}^*E^*}{\mathcal{L}(\omega)}. \tag{C13d}$$

The spectral density of the radiation pressure noise can be calculated using the same technique as in Appendix A, i.e.,

$$S_F(\Omega)=\frac{1}{2}[S_F'(\omega_0-\Omega)+S_F'(\omega_0+\Omega)], \tag{C14}$$

where

$$S_F'(\omega_0-\Omega)=4\hbar^2\kappa^2(\omega_0-\Omega)\times(|F_{a_s}^{\circlearrowleft}+F_{a_s}^{\circlearrowright}|^2+|F_{g_{s_{11}}}^{\circlearrowleft,I}+F_{g_{s_{11}}}^{\circlearrowright,I}|^2+|F_{g_{s_{21}}}^{\circlearrowleft,I}+F_{g_{s_{21}}}^{\circlearrowright,I}|^2+|F_{g_{s_{11}}}^{\circlearrowright,II}|^2+|F_{g_{s_{21}}}^{\circlearrowright,II}|^2). \tag{C15}$$

If one uses the formula (5) and the notation introduced in Table II, then it is easy to obtain that the radiation pressure noise spectral density in the narrowband approximation is defined by the following expression:

$$S_F(\Omega)=\frac{8\hbar\omega_0\tau W}{L^2}\frac{\gamma(1+\eta^2)(\gamma^2+\Omega^2)-2\gamma_1\eta(\gamma^2-\Omega^2)}{(1+\eta^2)(\gamma^2+\Omega^2)^2}, \tag{C16}$$

where $W=\hbar\omega_0|E|^2(1+\eta^2)/8$ is the light power at the end mirror.

5. Shot noise spectral density $S_x(\Omega)$

The shot noise spectral density can be obtained in the same manner as in Appendix A. Here

$$K(\Omega)=-\frac{2i\omega_0^{3/2}|E|}{c}\frac{e^{-i\Omega\tau}r_2t_1}{\mathcal{L}^2(\omega_0-\Omega)}[\mathcal{B}_1(\omega_0-\Omega)\sin\Psi-\eta\mathcal{L}(\omega_0-\Omega)\sin(\Phi+\Psi)], \tag{C17}$$

where $\Psi=\phi_{LO}+\arg C$, $\eta=|\boldsymbol{\eta}|$, $\Phi=\arg\boldsymbol{\eta}$, and the spectral density is defined by the following expression:

$$S_x(\Omega)=\frac{\omega_0}{|K(\Omega)|^2}=\frac{\hbar c^2}{32\omega_0 W}\frac{(1+\eta^2)|\mathcal{L}(\omega_0-\Omega)|^2}{r_2^2 t_1^2|\mathcal{B}_1(\omega_0-\Omega)\sin\Psi-\eta\mathcal{L}(\omega_0-\Omega)\sin(\Phi+\Psi)|^2}. \tag{C18}$$

Using the narrowband approximation defined by Eq. (5) and Table II, the following expression for S_x can be written if one suppose $\Phi=0$:

$$S_x(\Omega)=\frac{\hbar L^2}{32\omega_0\tau W}\frac{(1+\eta^2)(\gamma^2+\Omega^2)^2}{\gamma_1\sin^2\Psi\{[(1+\eta)\gamma-2\gamma_1]^2+(1+\eta)^2\Omega^2\}}, \tag{C19}$$

where $L=c\tau$.

6. Real scheme cross-correlation spectral density S_{xF}

It can be shown that the cross-correlation spectral density for the real speed meter scheme with optical losses is the same as for the ideal one, i.e.,

$$S_{xF}=-\frac{\hbar}{2}\cot\Psi. \tag{C20}$$

The above expression does not depend on frequency and is the same in the narrowband approximation.

APPENDIX D: NARROWBAND OPTIMIZATION OF ξ^2

In this section we will perform the optimization of the speed meter interferometer sensitivity at some fixed given frequency Ω_0. In this connection it seems convenient to introduce new dimensionless variables

$$\upsilon=\frac{\Omega}{\gamma},\quad \varepsilon=\frac{\gamma-\gamma_1}{\gamma}=\frac{\alpha}{\gamma},\quad P=\frac{16\omega_0\tau W}{mL^2\gamma^3},\quad A=\cot\Psi \tag{D1}$$

to rewrite Eq. (21) as

$$\xi^2=\frac{1}{2}\left[Pa+\frac{1+A^2}{P}b\right]+A, \tag{D2}$$

where

$$a=\frac{\varepsilon+\upsilon^2(2-\varepsilon)}{\upsilon^2(1+\upsilon^2)^2},\quad b=\frac{\upsilon^2(1+\upsilon^2)^2}{2(1-\varepsilon)(\varepsilon^2+\upsilon^2)}. \tag{D3}$$

Optimizing Eq. (D2) with respect to P and A, one can readily show that it reaches minimum at

$$P=\frac{b}{\sqrt{ab-1}}\quad\text{and}\quad A=-\frac{1}{\sqrt{ab-1}}, \tag{D4}$$

where a and b should be taken at frequency Ω_0. When substituted in Eq. (D2), these expressions will turn it into

$$\xi^2=\sqrt{ab-1}. \tag{D5}$$

The second step is the minimization of the above expression with respect to γ. Obviously, to obtain the optimal value of γ it is necessary to solve the equation

$$\frac{\partial K}{\partial\gamma}=0,$$

where $K=ab$. Here we should remember that $\varepsilon=\alpha/\gamma$ and $\upsilon=\Omega_0/\gamma$; then the above equation is transformed to

$$\varepsilon\frac{\partial K}{\partial\varepsilon}+\upsilon\frac{\partial K}{\partial\upsilon}=0,$$

which after simplification will be written as

$$\upsilon^2+2\varepsilon-1=\frac{\Omega_0^2}{\gamma^2}+2\frac{\alpha}{\gamma}-1=0. \tag{D6}$$

The positive solution of this equation is

$$\gamma_{opt}=\alpha+\sqrt{\alpha^2+\Omega_0^2}\simeq\Omega_0, \tag{D7}$$

where the last approximate equality corresponds to the case of small losses $\alpha\ll\Omega_0$. Substituting the obtained results in Eq. (D5) with respect to the case of small losses, one will have

$$\xi_{min}=\sqrt[4]{\frac{\varepsilon+\varepsilon^2-\varepsilon^3}{1-\varepsilon+\varepsilon^2-\varepsilon^3}}\simeq\sqrt[4]{\varepsilon}=\sqrt[4]{\frac{\alpha}{\Omega_0}}, \tag{D8}$$

which is the same expression that is presented in formula (22).

[1] V.B. Braginsky, Sov. Phys. JETP **26**, 831 (1968).

[2] Yu.I. Vorontsov and F.Ya. Khalili, Moscow Univ. Phys. Bull. **17**, 205 (1976).

[3] V.B. Braginsky, Yu.I. Vorontsov, and F.Ya. Khalili, Sov. Phys. JETP **46**, 705 (1977).

[4] K.S. Thorne, R.W.P. Drever, C.M. Caves, M. Zimmerman, and V.D. Sandberg, Phys. Rev. Lett. **40**, 667 (1978).

[5] Y.I. Vorontsov, *Theory and Methods of Macroscopic Measurements* (Nauka, Moscow, 1989).

[6] V.B. Braginsky and F.Ya. Khalili, *Quantum Measurement*

(Cambridge University Press, Cambridge, England, 1992).
[7] V.B. Braginsky and F.Ya. Khalili, Phys. Lett. A **147**, 251 (1990).
[8] F.Ya. Khalili and Yu. Levin, Phys. Rev. D **54**, 4735 (1996).
[9] V.B. Braginsky, M.L. Gorodetsky, F.Ya. Khalili, and K.S. Thorne, Phys. Rev. D **61**, 044002 (2000).
[10] P. Purdue, Phys. Rev. D **66**, 022001 (2002).
[11] Y. Chen and P. Purdue, Phys. Rev. D **66**, 122004 (2002).
[12] Y. Chen, Phys. Rev. D **67**, 122004 (2003).
[13] G. Sagnac, C. R. Hebd. Seances Acad. Sci. **95**, 1410 (1913).
[14] R.W.P. Drever, in *Gravitational Radiation*, edited by N. Deruelle and T. Piram (North-Holland, Amsterdam, 1983).
[15] K.-X. Sun, M.M. Fejer, E. Gustafson, and R.L. Byer, Phys. Rev. Lett. **76**, 3053 (1996).
[16] P. Beyersdorf, M.M. Fejer, and R.L. Byer, Opt. Lett. **24**, 1112 (1999).
[17] S. Traeger, P. Beyersdorf, L. Goddard, E. Gustafson, M.M. Fejer, and R.L. Byer, Opt. Lett. **25**, 722 (2000).
[18] S.P. Vyatchanin and E.A. Zubova, Phys. Lett. A **201**, 269 (1995).
[19] F.Ya. Khalili, gr-qc/0211088.
[20] S.P. Vyatchanin and A.Yu. Lavrenov, Phys. Lett. A **231**, 38 (1997).
[21] B. Huttner and S.M. Barnett, Phys. Rev. A **46**, 4306 (1992).
[22] T. Gruner and D.-G. Welsch, Phys. Rev. A **51**, 3246 (1995).
[23] L. Knöll, S. Scheel, E. Schmidt, D.-G. Welsch, and A.V. Chizhov, Phys. Rev. A **59**, 4716 (1999).
[24] H.J. Kimble, Yu. Levin, A.B. Matsko, K.S. Thorne, and S.P. Vyatchanin, Phys. Rev. D **65**, 022002 (2002).